STATISTICS, OPTIMIZATION AND INFORMATION COMPUTING
Stat., Optim. Inf. Comput., Vol. **15**, January 2026, pp 586–601.
Published online in International Academic Press (www.IAPress.org)

Mathematical Modeling of Carotid Bifurcation Stenosis as a Cause of Ischemic Stroke

Arif Fatahillah [1,*], Dzawawi Dimas Adani [1], Robiatul Adawiyah [1], Susi Setiawani [1], Rafiantika Megahnia Prihandini[1], Haci Mehmet Baskonus[2]

[1]*Department of Mathematics Education, Universitas Jember, Indonesia*
[2]*Faculty of Education, Harran University, Sanliurfa, Turkey*

Abstract This paper discusses ischemic stroke. This is the most common type. It occurs due to the blockage of blood supply to the brain. One of them is carotid bifurcation stenosis. We constructed a mathematical model to examine this. It employed the finite volume technique. We tested the variation of the risk with the form, thickness and position of the narrowing. We made comparisons of varied shapes. These were bell, cosine and elliptical. Narrowing levels that we tested were 60%, 70% , 80% , and 90%. The model equations were solved through the use of the SIMPLE algorithm. This was done using Python to determine stroke risk. Both cases provided detailed data of velocity and pressure, which was obtained by simulation. This presented the hemodynamic effect in a better way. Simulations of Computational Fluid Dynamics were also performed. These are simulated turbulent flow of blood in the carotid bifurcation. We used ANSYS FLUENT for this. We find that it is highly dangerous to narrow by 90%. It propels blood speed and pressure extremely beyond safety.

Keywords Ischemic stroke, Finite volume, Carotid bifurcation

DOI: 10.19139/soic-2310-5070-2596

1. Introduction

Ischemic stroke is when brain tissue does not get enough oxygen and food. This happens because plaque narrows or blocks the carotid bifurcation. This damages the brain [26, 9]. The carotid artery is the only blood vessel that splits into a bigger part. Because of this, blood flow in that bigger part becomes rough or uneven. This makes it easier for cholesterol and calcium to build up there [21]. Older people get this disease more often. But in some places, healthy people have less risk [1, 14]. The mortality rate from ischemic stroke in East Asia surpasses that observed in Western countries such as the United Kingdom and the United States [17]. Certain lifestyle habits, including smoking, high cholesterol levels, high fat and high salt diets, hypertension, and lack of exercise, are recognized as factors that increase the risk of ischemic stroke [18, 22].

The stenosis that causes ischemic stroke is primarily due to fatty plaque buildup. The development of fatty plaques tends to occur more frequently in geometrically vulnerable areas, such as the curvature of the carotid bifurcation in the common carotid artery [1, 21]. These plaques typically form an arc-like shape as they develop gradually through the accumulation of cholesterol on the arterial walls. In this study, the investigated stenosis shapes include bell-shaped, cosine-shaped, and elliptical, as they closely resemble real stenosis formations. In addition to the shape variations, stenosis thickness is also varied at 60%, 70%, 80%, and 90%.

Several other studies have focused on stenosis in the carotid bifurcation. Lopez et al. (2021) concluded that blood flow velocity increases while pressure decreases in the stenosed region [10]. Another study by Pinyo et al. (2021)

*Correspondence to: Arif Fatahillah (Email: arif.fkip@unej.ac.id). Department of Mathematics Education, Universitas Jember, Jalan Kalimantan 37, 68126, Jember, Jawa Timur, Indonesia

ISSN 2310-5070 (online) ISSN 2311-004X (print)

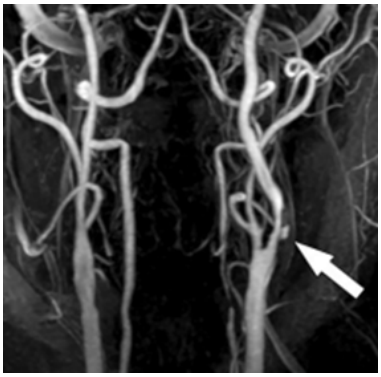

Figure 1. CT Scan of Carotid Bifurcation [15]

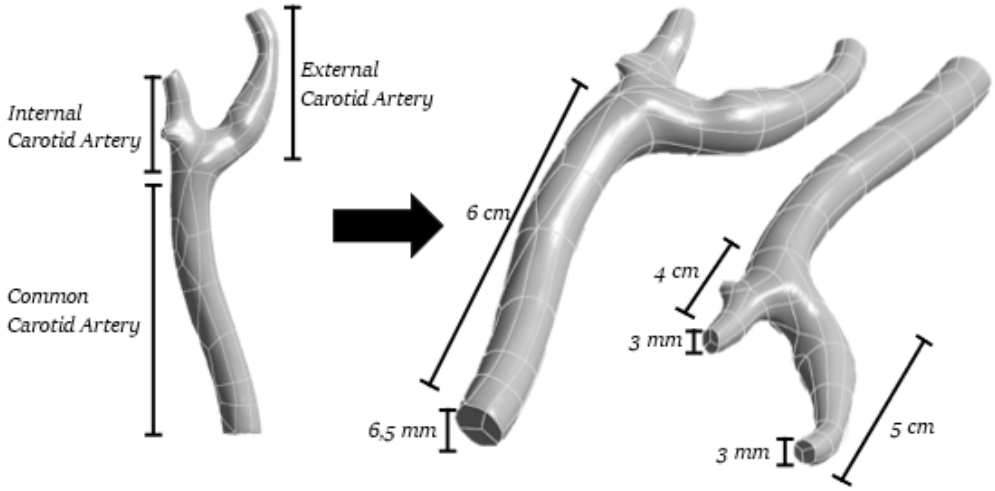

Figure 2. 3D Model of Carotid Bifurcation

examined a mathematical model of arterial stenosis with bell-shaped and cosine-shaped formations. They also found that uneven narrowing causes trickier blood flow patterns. The speed and pressure changes are more spread out because the blood flow is more spread out [20]. The study also showed that the blood moves fastest in the middle of the narrowed artery. Also, the speed in cosine-shaped narrowing is much lower than in bell-shaped narrowing. At the same time, Bhavya et al. (2024) looked at oval-shaped narrowing caused by radiation and chemicals. Their work also showed a math model with speed graphs and pictures to show the results [8]. The goal of this study is to look closely at how different shapes, thicknesses, and spots of narrowing change blood speed and pressure in the carotid bifurcation. We will do this by looking at the graphs and pictures we made.

2. Method

2.1. Mathematical Modeling

Several internal and external factors can contribute to vascular stenosis. This simulation aids medical researchers in understanding the internal factors that influence the narrowing of blood vessel walls. To analyze stenosis and identify its location, the stenosis shapes are studied, and diagrams are created, as shown in Figure 3. In this simulation, blood is considered a Newtonian fluid with incompressible, unsteady, and turbulent properties.

The fundamental equations governing the boundary conditions for simulating the blood flow hydrodynamics in the carotid bifurcation are defined as follows [16, 4, 25]:

Mass Conservation Equation

$$\nabla \cdot \vec{V} = 0 \tag{1}$$

Momentum Conservation Equation

$$\rho \left(\frac{\partial \vec{V}}{\partial t} + \left(\vec{V} \cdot \nabla \right) \vec{V} \right) = -\nabla p + \mu \nabla^2 \vec{V} \tag{2}$$

Sumit et al. (2023) [24] stated the boundary conditions for the stenosis radius in bell-shaped, cosine-shaped, and elliptical arterial stenosis as follows:

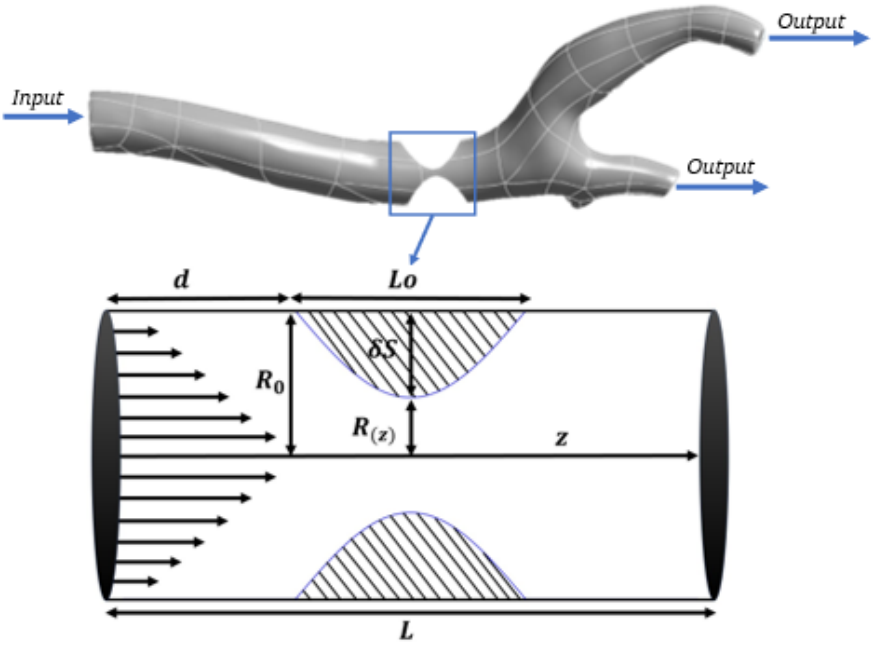

Figure 3. Blood Flow Geometry

Bell-Shaped equation:

$$\begin{cases} R(z) = R_0 - \delta_s e^{\frac{m_s^2}{R_0^2}\left(z - d - \frac{L_o}{2}\right)^2} & ; d \le z \le d + L_o \\ R(z) = R_0 & ; \text{otherwise.} \end{cases} \tag{3}$$

Cosine-Shaped equation:

$$\begin{cases} R(z) = R_0 - \frac{\delta_s}{2}\left(1 + \cos\frac{2\pi}{L_o}\left(z - d - \frac{L_o}{2}\right)\right) & ; d \le z \le d + L_o \\ R(z) = R_0 & ; \text{otherwise.} \end{cases} \tag{4}$$

Elliptical equation:

$$\begin{cases} R(z) = R_0 - \delta_s \sin\left(\frac{\pi(z-d)}{L_o}\right) & ; d_1 \le z \le d_1 + L_o \\ R(z) = R_0 & ; \text{otherwise.} \end{cases} \tag{5}$$

With:

$R(z)$ = radius on stenosis
R_0 = the arterial radius
δ_s = the maximum height of the stenosis
L = the arterial length
L_0 = the total length of the stenosis
z = flow direction
d = stenosis location
$u = v = 0$; at the arterial wall $(r = R(z))$

In the study by Roy et al. (2017), the inlet velocity values are as follows [19]:

$$u = 2U_0 \left(1 - \left(\frac{r}{R(z)}\right)^2\right) \quad ; \text{ at the inlet } (x = 0) \tag{6}$$

In Figure 3, R(z) represents the stenosis geometry, which can be mathematically expressed as:

$$R(z) = R_0 \left(1 - \delta e^{-\alpha\left(\frac{x}{R_0}\right)^2}\right) \tag{7}$$

R_0 represents the radius of the normal section of the artery, δ is the maximum height of the stenosis, and α is the stenosis shape parameter.

2.2. Discretization

The speed and pressure are found by solving the mass and momentum conservation equations (Equations 2.1 and 2.2). We use the Finite Volume Method to discretize these equations. This method is common in fluid dynamics studies [12, 2]. We chose it because it is reliable for accurate solutions. It is also effective for modeling blood flow [7, 10]. We used the SIMPLE algorithm. This algorithm handles the linked nature of the fluid flow equations. It is a standard technique in Computational Fluid Dynamics. It solves the basic pressure-velocity relationships. This makes it suitable for our simulation [13, 3, 5, 6].

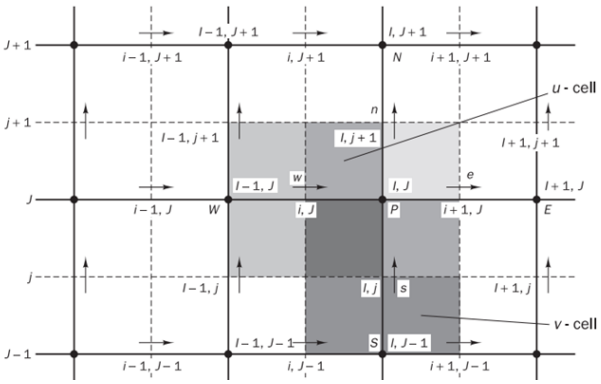

Figure 4. Discretization Scheme of the SIMPLE Algorithm [12]

The steps of the SIMPLE (Semi-Implicit Method for Pressure-Linked Equations) algorithm are as follows: [12, 3]:

1. Initializing Initial Guesses p^*, u^*, v^* dan ϕ^*.
2. Solving the Discretized Momentum Equations

$$a_{i,j}u^*_{i,j} = \sum a_{nb}u^*_{nb} + \left(p^*_{i-1,j} - p^*_{i,j}\right)A_{i,j} + b_{i,j}$$

$$a_{i,j}u^*_{i,j} = \sum a_{nb}u^*_{nb} + \left(p^*_{i,j-1} - p^*_{i,j}\right)A_{i,j} + b_{i,j}$$

3. Solving the Pressure Correction Equation

$$a_{I,J}p'_{I,J} = a_{I+1,J}p'_{I+1,J} + a_{I-1,J}p'_{I-1,J} + a_{I,J+1}p'_{I,J+1} + a_{I,J-1}p'_{I,J-1} + b'_{I,J}$$

4. Determining the Corrected Pressure and Velocity

$$u'_{i+1,j} = u^*_{i+1,j} + d_{i+1,j}\left(p'_{I,J} - p'_{I+1,J}\right)$$

$$v'_{i,j+1} = v^*_{i,j+1} + d_{I,j+1}\left(p'_{I,J} - p'_{I,J+1}\right)$$

Where,

$$d_{i+1,j} = \frac{A_{i+1,j}}{a_{i+1,j}} \quad \text{and} \quad d_{i,j+1} = \frac{A_{i,j+1}}{a_{i,j+1}}$$

5. Solving All Other Discretized Transport Equations

$$a_{I,J}\phi_{I,J} = a_{I+1,J}\phi_{I+1,J} + a_{I-1,J}\phi_{I-1,J} + a_{I,J+1}\phi_{I,J+1} + a_{I,J-1}\phi_{I,J-1}$$

Check whether the discretized solution has converged. If not, repeat Steps 1–4 until convergence is achieved.

The next step is to change the blood vessel shape into simple math equations. And Python is used to solve them. We use ANSYS Fluent to look at the fluid flow in the vessel. So, we divide the space into many small cells. Then, the software finds the speed and pressure in the center of each cell. The program repeats the math until the answer is stable. The time step is 0.1 seconds, and the test runs for 200 steps.

2.3. Simulation Parameters

Table 1 presents the factors affecting blood flow rate in the carotid bifurcation due to vascular stenosis [7, 11, 19, 23, 27]. A numerical experiment was conducted to analyze blood flow through a stenotic artery with blockage levels of 60%, 70%, 80%, and 90%.

Table 1. Value of Parameter Factors Affecting Blood Flow Rate

Parameter	**Value**
Diameter of *carotid bifurcation*	6,5 mm
Blood Density	1060 kg/m^3
Viscosity	0,0035 kg/ms
Flow Velocity	0,5 m/s
Pressure	15998.64 Pa

3. Results and Discussion

3.1. Results

The numerical analysis of the carotid bifurcation blood vessel as a cause of ischemic stroke was done by checking the simulation results from the mathematical model using Python and the geometric design simulation using Fluent. In Figure 5, for bell-shaped stenosis, blood flow velocity goes up as the stenosis percentage goes up. At 45% stenosis, the velocity increase is still small (yellow-green area). But, at 90% stenosis, a very big jump in velocity is seen (orange-red area at the stenosis center). The velocity change rate gets stronger as the narrowing gets bigger, so the risk of the artery wall tearing goes up.In Figure 6, for cosine-shaped stenosis, the diameter change follows a cosine function. At 60% and 70% stenosis, the fastest velocity is only at the narrowest spot. At 80% and 90% stenosis, a very big velocity spike shows up in the middle stenosis area (red area), and the velocity is spread out more evenly. The velocity change rate gets stronger, especially where the stenosis is at its peak.In Figure 7, for elliptical-shaped stenosis, the inlet and

outlet diameter changes are like the other shapes, but the stenosis peak is more round. The flow velocity goes up as the stenosis percentage goes up. At 60% and 70% stenosis, the velocity pattern is more steady than the other stenosis shapes. But, at 80% and 90% stenosis, the peak velocity goes up fast at the narrowest spot. This happens because of the elliptical shape, which gives a more steady flow before it hits the biggest stenosis area.

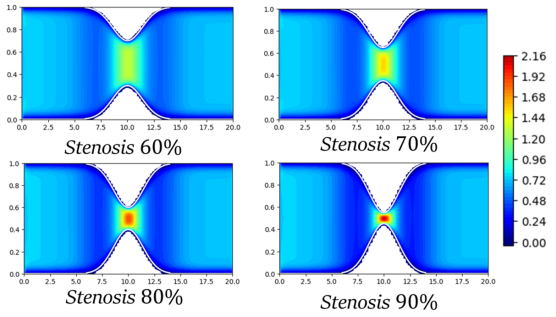

Figure 5. Bell-shaped model with varying stenosis thickness

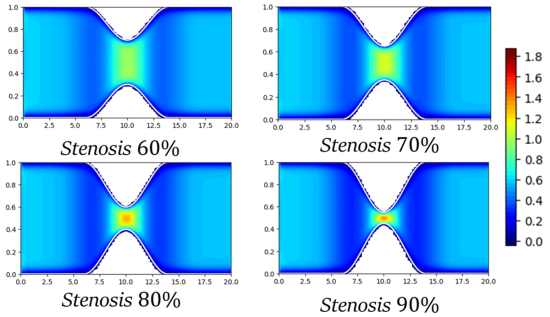

Figure 6. Cosine-shaped model with varying stenosis thickness

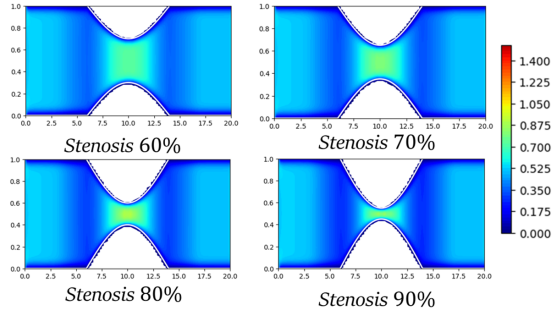

Figure 7. Elliptical model with varying stenosis thickness

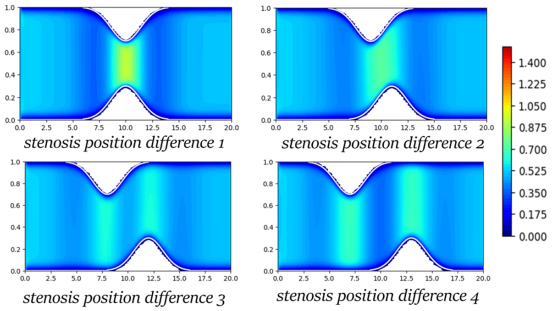

Figure 8. Bell-shaped model with varying stenosis locations

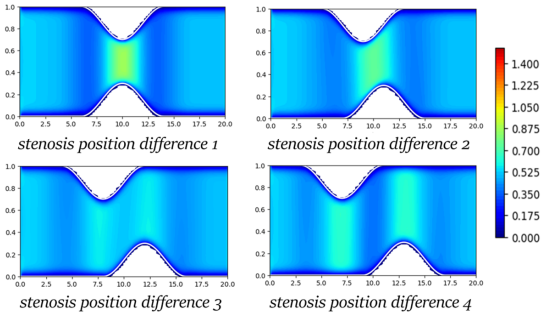

Figure 9. Cosine-shaped model with varying stenosis locations

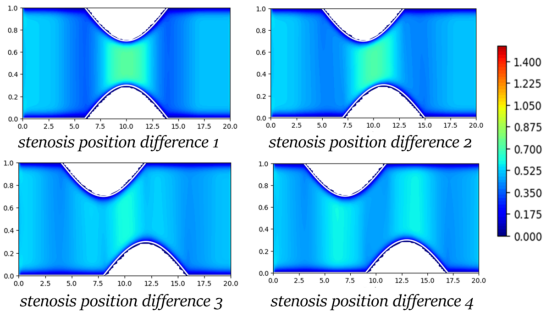

Figure 10. Elliptical model with varying stenosis locations

Patterns These patterns of velocity differ among the shapes. Figure 8 the bell-shaped model the region of high velocities would be very concentrated on the peak. This is a junction of sudden flow restriction. Downstream, the flow expands. This is demonstrated with the change to green and blue color. Velocity accumulation develops with the

position of stenosis. A more distal location of stenosis forms a longer adaption zone of the fluid prior to acceleration. This causes the flow pattern to change. In the cosine-shaped model of figure 9, there is a massive blue area to the downstream of the model that is characterized by a strong deceleration of the flow. The increase in velocities still remains to be dependent on stenosis location. There is a smooth change of blue towards green on the contour lines. This distribution indicates a less volatile and progressive velocity distribution. The model shown in figure 10, which is elliptical-shaped, creates an instantaneous narrowing of the flow at the stenosis. It creates an otherwise high-velocity zone on the forefront. The expansion of the flow and the decrease of the velocity is evident as the green-blue colors occur after that in the stream. There is a also loss in the point of maximum velocity which varies with the location of stenosis. Further downstream stenosis gives more time to length of adaptation before acceleration. This has a direct effect on the end velocity profile.

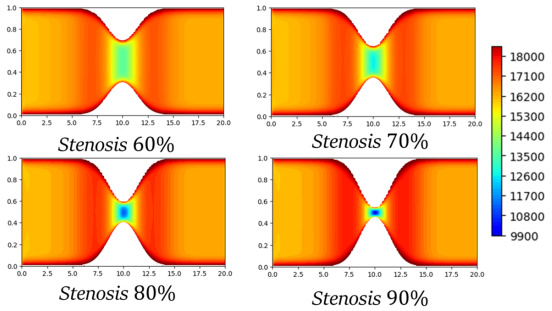

Figure 11. Bell-shaped model with varying stenosis thickness

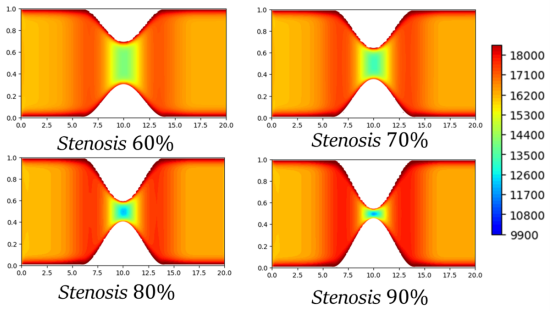

Figure 12. Cosine-shaped model with varying stenosis thickness

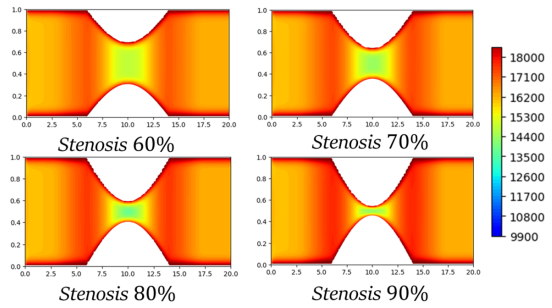

Figure 13. Elliptical model with varying stenosis thickness

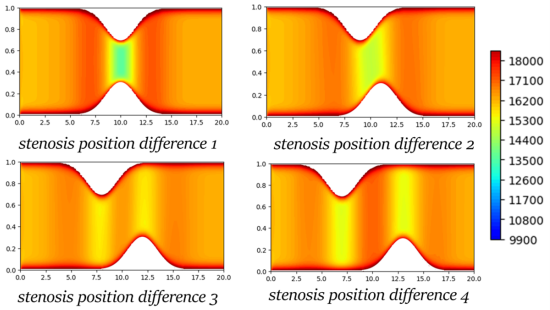

Figure 14. Bell-shaped model with varying stenosis locations

In Figure 11, for the bell-shaped model, at 60% stenosis, the pressure remains uniform with a slight decrease at the narrowest region (light green). At 70% stenosis, the pressure drop becomes more pronounced (yellow-green area). At 80% stenosis, a blue zone begins to appear in the stenotic region, indicating low pressure due to increased velocity. At 90% stenosis, the blue area expands and intensifies, showing the most extreme pressure drop, with a sharp contrast between the inlet (red) and the stenotic zone (blue). For the cosine-shaped model, the pressure pattern is like the bell-shaped stenosis. At 60% stenosis, the pressure is mostly the same. At 70% stenosis, the pressure drop in the middle area is clearer, but the low-pressure (blue) zone is not yet the main feature. At 80% stenosis, a blue zone appears, which means low pressure, and there is a big difference between the entry point (red-orange) and the stenosis area (blue). At 90% stenosis, the blue area gets stronger, showing a very large pressure drop because the flow speeds up a lot.For the elliptical-shaped model, at 60% stenosis, the pressure drop in the narrowed area is still very small (yellow-green area). At 70% stenosis, the pressure drop is easier to see in the middle area (green zone). At 80% stenosis, the pressure pattern is almost the same as at 70% stenosis. At 90% stenosis, the yellow area extends around the stenosis, indicating

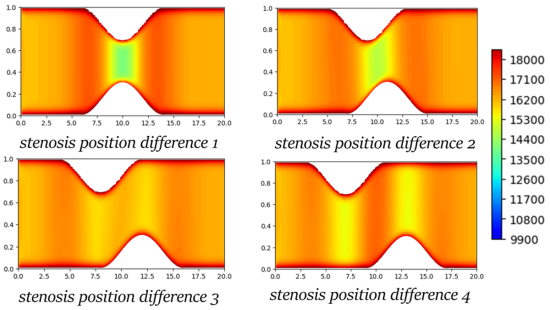

Figure 15. Cosine-shaped model with varying stenosis locations

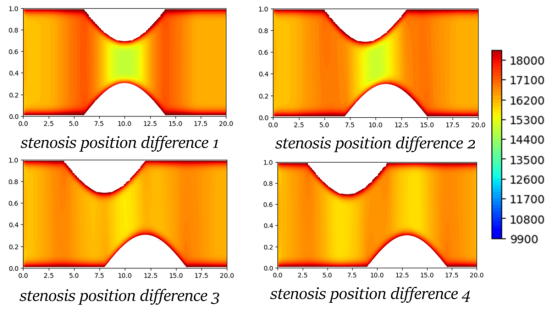

Figure 16. Elliptical model with varying stenosis locations

an increase in velocity and a corresponding pressure drop, though it is less intense compared to the other stenosis shapes.

In Figure 14, the bell-shaped model illustrates the effect of stenosis position on pressure distribution in bell-shaped stenosis. In Position 1, stenosis in the center creates a low-pressure region (yellow-green) around the stenosis peak. In Position 2, the low-pressure area is concentrated in the middle of the channel, with a more uniform pressure gradient. In Position 3, the pressure remains relatively high, dominated by orange-red colors. In Position 4, stenosis at the end of the channel causes high pressure to be more evenly distributed. In Figure 15, the cosine-shaped model shows how where the blockage is affects the pressure distribution for a cosine-shaped blockage. In Position 1, the blockage in the center makes the pressure low at the highest point of the blockage. In Position 2, the low pressure is only in the middle of the channel, and the pressure change is more even. In Position 3, the pressure stays quite high, so orange-red colors are mostly seen. In Position 4, the blockage at the end makes the pressure distribution more the same, and the pressure stays high. In Figure 16, the elliptical-shaped model shows how where the blockage is affects the pressure distribution in an elliptical blockage. In Position 1, with the blockage in the center, low pressure shows up at the highest point of the blockage. In Position 2, the low-pressure area is only in the middle of the channel. The pressure change is still big, but it is more spread out because the elliptical shape is smooth. In Position 3, the pressure lines show a medium pressure drop, and orange-red areas are still mostly seen. Then, in Position 4, where the blockage is at the end, the pressure stays high, as the pressure caused by the blockage is spread evenly across the flow.

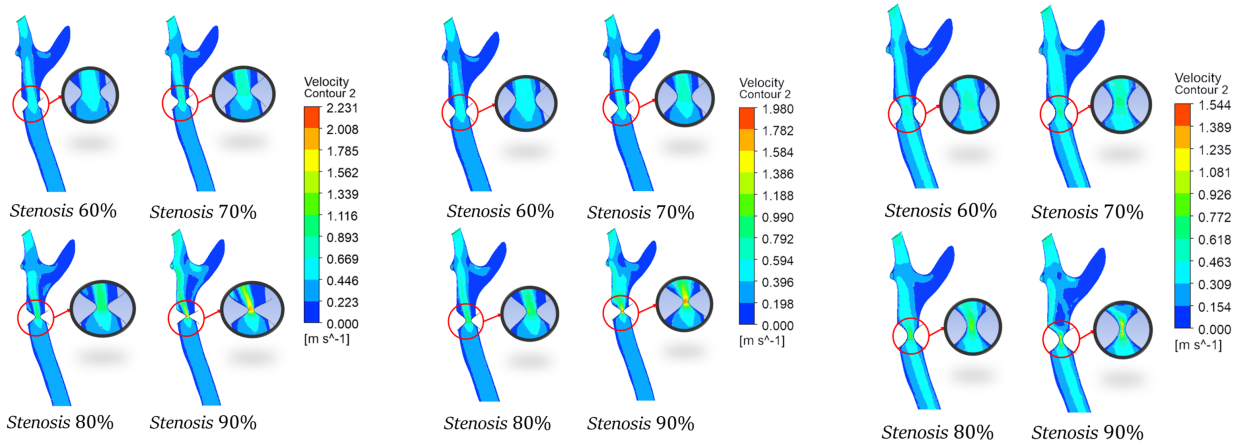

Figure 17. Simulation Results of Velocity in Ansys with Varying Stenosis Thickness

Side by side comparison of the three stenosis models that are bell-shaped, cosine-shaped and elliptical in the carotid bifurcation are shown in figure 17. In the bell-shaped model, a blue zone as the prevalent area at 60% stenosis of the

bell represents low flow velocity. When the stenosis reaches 70 and 80, an enlargement of green-yellow areas in the area of constriction emphasizes a significant increase in velocity. This tendency reaches its peak at 90% stenosis, when the local yellow-red hues at the point of minimum allow to imagine the dangerously high velocities. Cosine shaped model shows the distribution of velocity that resembles its smooth, geometric narrowing. With stenosis of 60% the low velocity is visible due to the remarkable blue area. At 70 percent and 80 percent, the development of green zones at the stenosis area is an indication of increasing flow. The most extreme constriction is 90% stenosis, which puts the peak velocity at the center, and that is observed through bright yellow-red colors. Widespread blue depicts low initial velocity at 60% stenosis in the elliptical-shaped model. The acceleration of the velocity becomes obvious at 70% stenosis when green areas appear. A major jump in velocity is characterized by an enlarged area on green-yellow at 80% stenosis. Lastly, when stenosis is 90%, the flow is at its peak, and the yellow-red areas prevail on the slimmest part of the vessel.

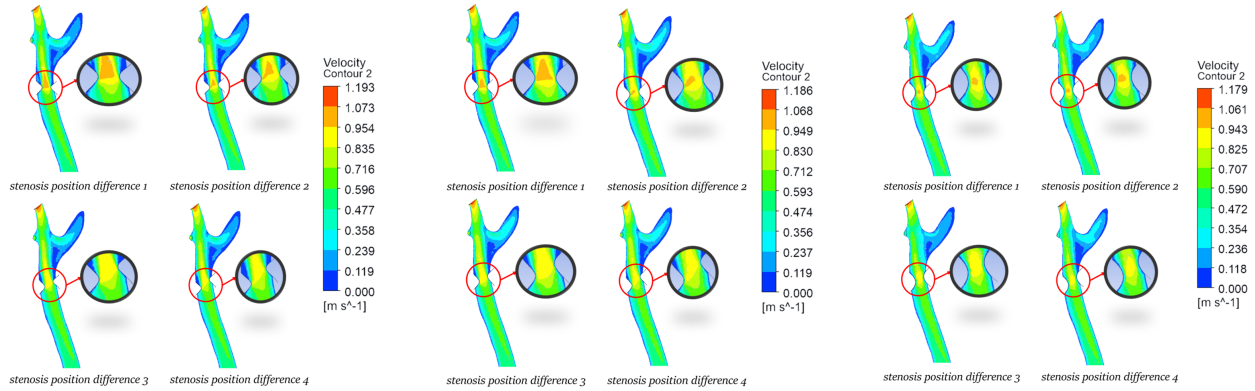

Figure 18. Simulation Results of Velocity in Ansys with Varying Stenosis Locations

In Figure 18, it is shown that the farther the stenosis location, the smaller its impact on velocity increase. This can be observed from Position 1 to Position 4, where the maximum flow velocity tends to decrease due to a more evenly distributed flow. As a result, the acceleration at the stenosis point becomes lower.

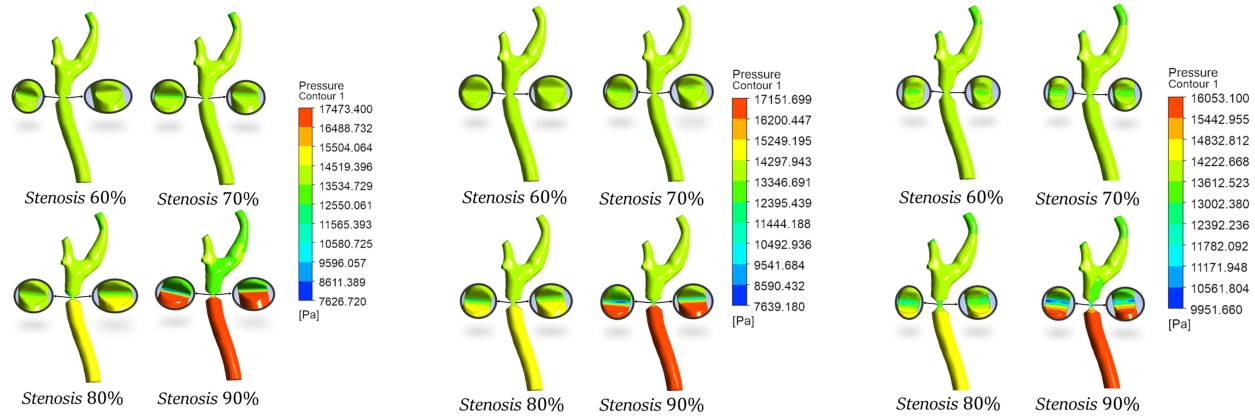

Figure 19. Simulation Results of Pressure in Ansys with Varying Stenosis Thickness

Figure 19 shows the pressure distributions for the three stenosis models. They are shown at the same severity levels. In the bell-shaped model, pressure is mostly uniform and moderate at 60% stenosis. A noticeable decrease begins at 70%. The stenotic area turns a darker green. This drop becomes more pronounced at 80%. Pressures approach

the lower, blue range of the scale. The most extreme drop occurs at 90% stenosis. Green-blue colors show the point of minimum pressure at the narrowest section. A sharp rise in pressure happens just before the stenosis as severity increases. This is caused by flow resistance. It is paired with a severe drop within the constriction itself. The cosine-shaped model shows a comparable trend. Pressures stay relatively stable and uniform for both 60% and 70% stenosis. A more significant decline becomes apparent at 80%. Values near the blue range. The 90% stenosis case results in the lowest observed pressure. The narrowed region is dominated by green-blue tones. Results for the elliptical-shaped model align with this pattern. A uniform green field at 60% stenosis indicates steady pressure. A decrease commences at 70%. It intensifies at 80% as pressures approach blue levels. The minimum pressure is again localized at the narrowest point for the 90% case. This is shown by dominant green-blue colors.

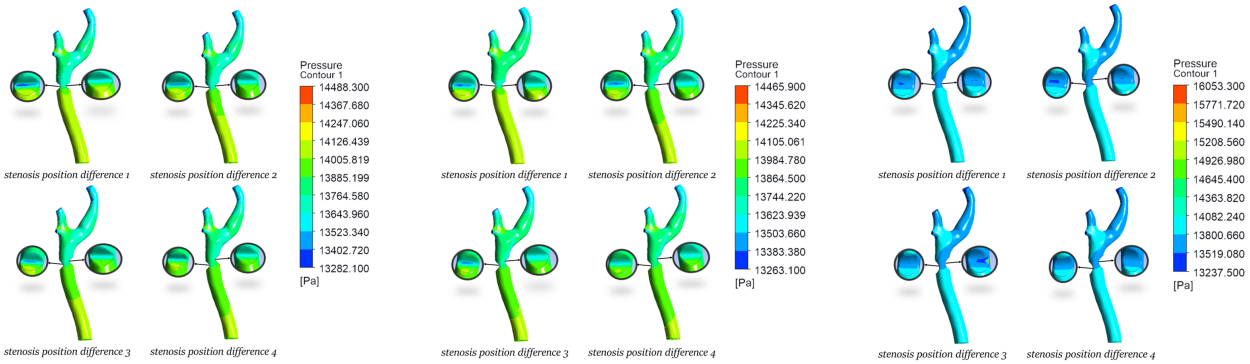

Figure 20. Simulation Results of Pressure in Ansys with Varying Stenosis Locations

In Figure 20, it is shown that the farther the stenosis location, the smaller its impact on pressure reduction. From Position 1 to Position 4, the pressure drop is not significant. Different stenosis positions result in a more uniform pressure distribution, leading to higher overall pressure compared to symmetrical stenosis with the same cross-sectional area.

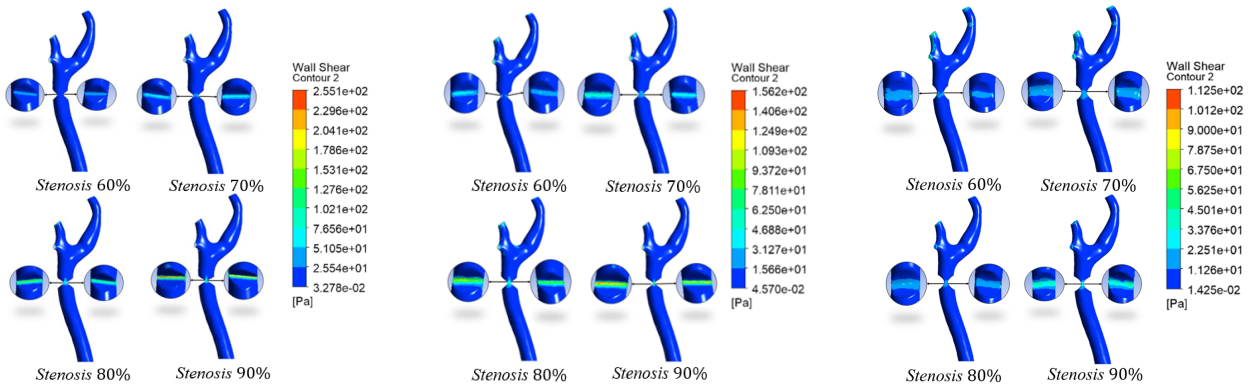

Figure 21. The simulation results of wall shear stress (WSS)

Figure 21 illustrates the wall shear stress (WSS) distribution at different levels of stenosis severity (60%–90%). As the degree of narrowing increases, the maximum WSS values tend to rise and become more concentrated around the most constricted regions. These high-WSS areas may impose significant mechanical stress on the arterial wall. This can lead to plaque instability and increase the risk of rupture.

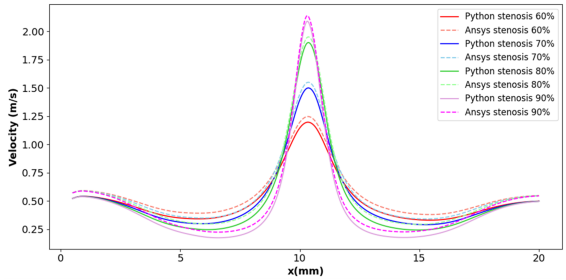

Figure 22. Velocity graph of a bell-shaped model with varying stenosis thickness

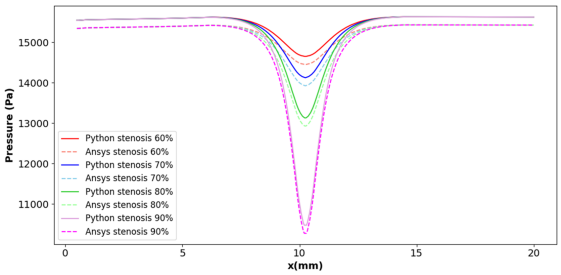

Figure 23. Pressure graph of a bell-shaped model with varying stenosis thickness

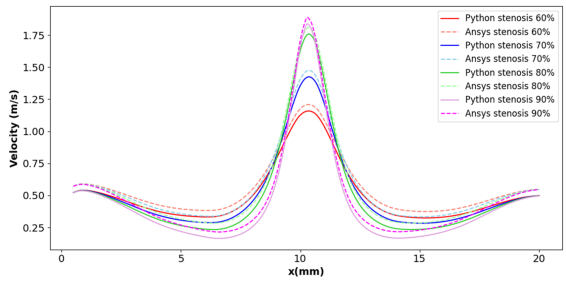

Figure 24. Velocity graph of a cosine-shaped model with varying stenosis thickness

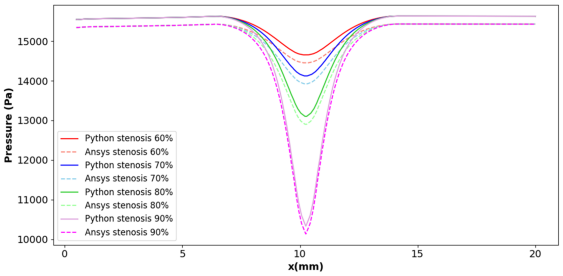

Figure 25. Pressure graph of a cosine-shaped model with varying stenosis thickness

3.2. Discussion

The graphs in Figures 22 to 27 present the simulation results using Python and Fluent, considering different stenosis thicknesses in the carotid bifurcation. These graphs indicate that before reaching the stenotic region, the blood pressure tends to be high, then gradually decreases towards the stenosis center. Conversely, the flow velocity is initially low but increases as it approaches the stenotic center. Beyond the stenotic region, pressure rises again as the flow cross-sectional area increases, while velocity decreases. These findings align with the study by Lopez et al. [10], which reported that blood pressure before stenosis tends to be high and subsequently drops toward the stenosis center, while flow velocity increases in the narrowing region and has the same flow pattern and stenosis effect as the study by S. Kumar et al 2023 [24]. Furthermore, the data reveal that among the three stenosis models analyzed (bell-shaped, cosine-shaped, and elliptical), the bell-shaped model has the most significant impact on velocity and pressure changes. These results support the findings of Pinyo et al. (2021) and Bhavya et al. [8, 20], which stated that the bell-shaped stenosis leads to a more significant velocity increase and a sharper pressure drop in the stenotic region compared to other shapes.

Table 2. Comparison of Peak Velocity and Peak Pressure for Bell-Shaped Stenosis at Different Mesh Sizes.

Mesh Size	**Number of Nodes**	**Peak Velocity**		**%Difference**	**Peak Pressure Drop**		**%Difference**
		MATLAB	**ANSYS**		**MATLAB**	**ANSYS**	
Coarse Mesh	75702	2.076	2.231	7.19%	9820.138	10420.14	5.92%
Medium Mesh	163891	2.054	2.160	5.03%	9880.15	10220.12	3.38%
Fine Mesh	309720	2.048	2.089	1.98%	9910.23	10017.91	1.08%

We conducted grid independence study to check our simulation results. We made a comparison between the computed peak velocity and peak pressure drop. There were three mesh densities coarse, medium and fine that we

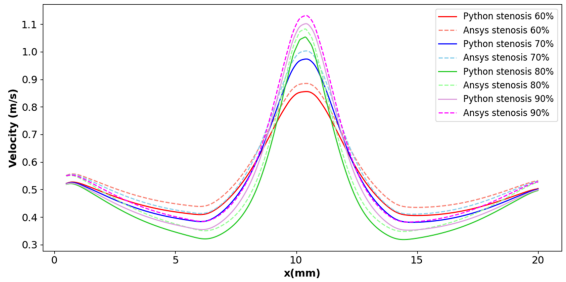

Figure 26. Velocity graph of a elliptical model with varying stenosis thickness

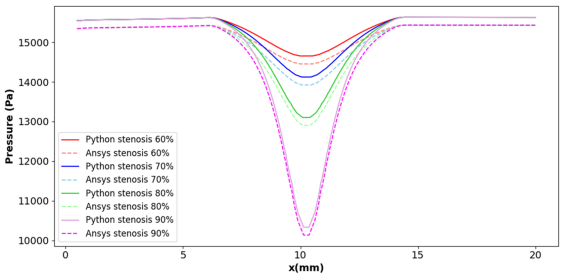

Figure 27. Pressure graph of a elliptical model with varying stenosis thickness

Table 3. Comparison of Peak Velocity and Peak Pressure for Cosine-Shaped Stenosis at Different Mesh Sizes.

Mesh Size	**Number of Nodes**	**Peak Velocity**		**%Difference**	**Peak Pressure Drop**		**%Difference**
		MATLAB	**ANSYS**		**MATLAB**	**ANSYS**	
Coarse Mesh	75702	1.697	1.802	6.00%	10526.12	10989.341	4.30%
Medium Mesh	163891	1.721	1.787	3.76%	10646.172	10889.282	2.25%
Fine Mesh	309720	1.741	1.767	1.48%	10734.784	10878,142	1.32%

Table 4. Comparison of Peak Velocity and Peak Pressure for Elliptical Stenosis at Different Mesh Sizes.

Mesh Size	**Number of Nodes**	**Peak Velocity**		**%Difference**	**Peak Pressure Drop**		**%Difference**
		MATLAB	**ANSYS**		**MATLAB**	**ANSYS**	
Coarse Mesh	75702	0.987	1.048	5.99%	13372.132	14140.563	5.58%
Medium Mesh	163891	0.988	1.024	3.57%	13433.113	13940.593	3.70%
Fine Mesh	309720	0.991	1.005	1.40%	13197.137	13640.165	1.05%

used. These comparisons are described in Tables 2-4 according to the stenosis shapes. The data indicate that the more the mesh is refined into a fine one the greater the percentage difference between the MATLAB and ANSYS results becomes consistent. This disparity is also reduced. This tendency proves the fact that convergence has been created with the help of the numerical solution. Our choice of the fine mesh setting was made in the rest of the simulations. This ensures correctness and dependability of our findings.

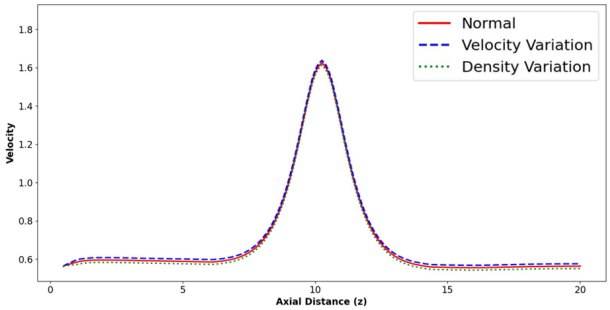

Figure 28. Comparison of Blood Flow Velocity Profiles for Three Scenarios

Figure 28 shows how the blood flow velocity profile changes along the axial direction. It shows three distinct conditions. The normal scenario is shown by the red solid line. The blue dashed line shows the effect of varying the initial velocity input. The green dotted line tracks the influence of altering the fluid density. This comparison demonstrates that the simulation accounts for uncertainty in key inputs. Variations in initial velocity and blood density can occur in vivo. These variations are shown to influence the precise hemodynamic outcome. These parameter changes introduce slight deviations in the velocity profile. The core flow pattern remains fundamentally consistent across all three scenarios.

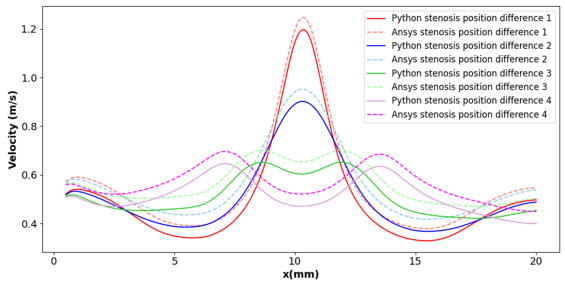

Figure 29. Velocity graph of a bell-shaped model with varying stenosis location

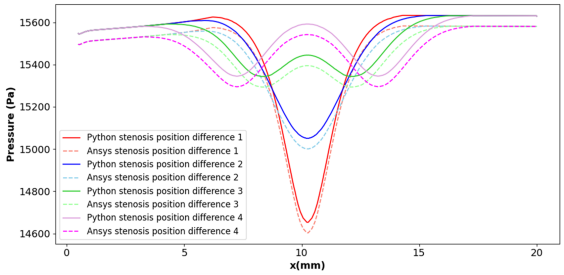

Figure 30. Pressure graph of a bell-shaped model with varying stenosis location

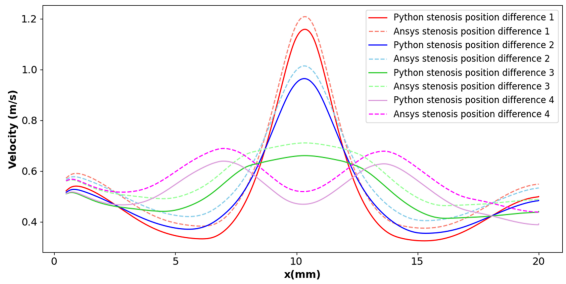

Figure 31. Velocity graph of a cosine-shaped model with varying stenosis location

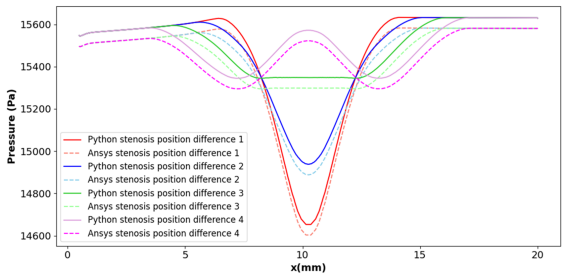

Figure 32. Pressure graph of a cosine-shaped model with varying stenosis location

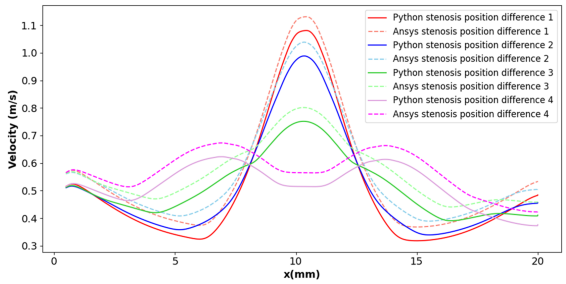

Figure 33. Velocity graph of a elliptical model with varying stenosis location

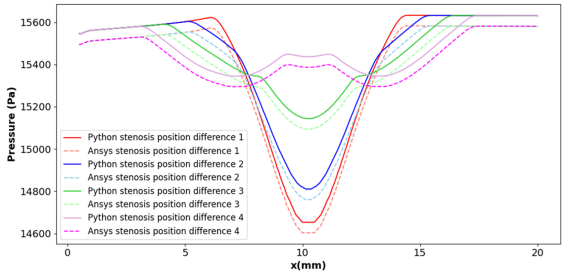

Figure 34. Pressure graph of a elliptical model with varying stenosis location

Resulting figures 28 to 33 indicate the outcomes of the Python and Fluent simulations. They demonstrate the effect of stenosis site on fluid flow. A clear trend emerges. As the location of the stenosis increases distance to the origin of the vessel, the impact of this location on raising the velocity of flow reduces. This occurs due to a further distal stenosis where the flow can be developed more uniformly in front of the hindrance. The resultant velocity profile is

less and more homogenous. Less area is covered by dissipation of the kinetic energy of the fluid. On the contrary, the flow is funnelled and concentrated by a thicker or more symmetrical stenosis near the first point. This results in more localized and intense spike velocity.

Table 5. Flow Velocity and Pressure Data for the Three Shape Models

Shape of Stenosis	**Thickness Level (%)**	**Velocity (m/s) / Pressure (Pa)**
Bell-shaped	60%	1 – 1,2 / 14300 – 15200
	70%	1,4 – 1,6 / 13400 – 14300
	80%	1,8 – 2 / 11600 – 13400
	90%	2 – 2,1 / 9800 – 10700
Cosine-shaped	60%	1 – 1,1 / 14300 – 15200
	70%	1,1 – 1,2 / 13400 – 14300
	80%	1,3 – 1,6 / 12000 – 14000
	90%	1,6 – 1,8 / 10000 – 11000
Elliptical	60%	0,525 – 0,7 / 14300 – 15200
	70%	0,7 – 0,85 / 13400 – 14300
	80%	0,85 – 0,9 / 13400 – 14400
	90%	0,85 – 1,050 / 13200 – 14200

Figure 35 tracks plaque progression in the carotid artery over 5, 10, and 15-year intervals. The visualization reveals a clear trend of increasing arterial narrowing over time. Plaque accumulates within the lumen. This progressive constriction is marked by an intensifying red zone at the stenosis site. The growing prominence of this area represents a rise in local blood flow velocity. Velocity escalates as the vessel becomes more severely obstructed.

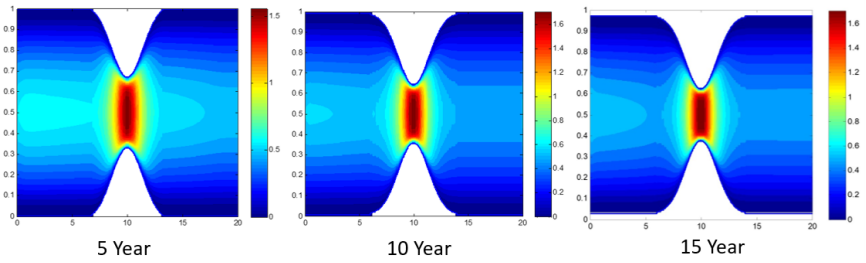

Figure 35. Evolution of Stenosis Growth

The findings of the simulation have indicated two things. To start with, stenoses with greater thickness and symmetry result in a higher velocity of flow increase. Stenoses that are more distant to the vessel origin result in a lesser increase. Second, the distribution of pressure is significantly changed by the position of the stenosis. A more distal stenosis has a lesser impact on pressure reduction. This lesser pressure drop is attributed to the fact that there is more room to develop the flow. This results in more balanced distribution of pressure. It averts severe local falls. A stenosis that is more focused and severe is produced by a thicker, symmetrical stenosis. Constriction causes the flow to be immensely concentrated. This causes an increased and sharper pressure gradient.

The discussion validates that the hemodynamic risk is dependent on stenosis geometry. The more symmetrical and thicker constriction creates the worst conditions. It leads to a significant increase in the velocity of flow. It also leads to sharp decrease in pressure. This interaction initiates high wall shear stress. This is a mechanical stress that is damaging of the vessel lining. This profile of stenosis is a much worse environment than other shapes or the more distal location. These results indicate that the form and location of a stenosis have a significant influence on the flow patterns. They have a direct effect on the conditions that might stimulate the plaque formation and progression.

4. Conclusion

This study simulated stenosis within the carotid bifurcation to assess its role in ischemic stroke risk, specifically analyzing resulting changes in blood flow behavior. The work also validated a mathematical model of this flow for three stenosis profiles—bell-shaped, cosine-shaped, and elliptical—across a range of severities from 60% to 90% narrowing. The principal outcomes are summarized as follows:

- The findings of both the numerical simulations and the CFD indicate the same fact. A stenosis of 90 per cent is a life-threatening risk in the carotid bifurcation. This applies to all particular shapes. This condition creates extreme forces of hemodynamics that place a high risk. This is the danger of developing arterial rupture or damage.
- The trend of the simulations is evident. The velocity of flow and pressure drop increase gradually with the increase in the thickness of stenosis. This direct association highlights a serious requirement. Medical treatment should be done early. The earlier the stenosis is detected and addressed at a lower scale, the better the outcome can be achieved. It will be able to avoid serious complications.
- The hemodynamic effect of a stenosis is also determined by the location. A stenosis that is asymmetrically located produces a lesser impact on the local velocity and pressure. The reason behind this is that the flow possesses a direction to spread the flow more equally around the obstruction. This will eliminate a severe, localized pressure accretion.

Acknowledgement

This research is supported by the Computational Research Group and Virtual Laboratory, Department of Mathematics Education, University of Jember, Jember, Indonesia

REFERENCES

1. Ali Müftüoğulları and Münir Süner and Buğra Sarper The effect of bifurcation angulation on flow characteristics and hemodynamic indicators in an idealized left coronary artery. *International Journal of Thermofluids* 2024. P. 100554. 10.1016/j.ijft.2023.100554
2. Anley, E. F. Numerical Solutions of Elliptic Partial Differential Equations by Using Finite Volume Method. *Pure and Applied Mathematics Journal* 2016. Vol. 5. 10.11648/J.PAMJ.20160504.16
3. Arif Fatahillah, Basuki Widodo, Rozaini Roslan Mathematical modeling of Ischaemic central retinal vein occlusion using finite volume method. *AIP Conf. Proc.* 2024. 10.1063/5.0222460
4. A Fatahillah, B Widodo, R Roslan The Modeling and Numerical Solution of Branch Retinal Artery Occlusion. *Malaysian Journal of Mathematical Sciences* 2025. Vol. 19 10.47836/mjms.19.1.01
5. Arif Fatahillah, Dimas Agung Prasetyo, Robiatul Adawiyah, Susi Setiawani, Arika Indah Kristiana Numerical modelling of blood vessel constriction due to peripheral artery disease using finite volume method. *AIP Conf. Proc.* 2024. 10.1063/5.0222462
6. Attar, H., Ahmed, T., Rabie, R., Amer, A., Khosravi, M. R., Solyman, A., & Deif, M. A. Modeling and computational fluid dynamics simulation of blood flow behavior based on MRI and CT for Atherosclerosis in Carotid Artery. *Multimedia Tools and Applications* 2024. Vol. 83. 10.1007/s11042-023-17765-w
7. A. Ostadfar Chapter 1 - Fluid Mechanics and Biofluids Principles. *Academic Press* 2016. P. 1–60. 10.1016/B978-0-12-802408-9.00001-6
8. B. Tripathi and B. K. Sharma Two-phase analysis of blood flow through a stenosed artery with the effects of chemical reaction and radiation. *Ricerche mat* 2024. Vol. 73 P. 151–177. 10.1007/s11587-021-00571-7
9. Costa D, Scalise E, Ielapi N, Bracale UM, Faga T, Michael A, Andreucci M, Serra R. Omics Science and Social Aspects in Detecting Biomarkers for Diagnosis, Risk Prediction, and Outcomes of Carotid Stenosis. *Biomolecules* 2024. Vol. 8 10.3390/biom14080972
10. D. Lopes and R. Agujetas and H. Puga and J. Teixeira and R. Lima and J.P. Alejo and C. Ferrera Analysis of finite element and finite volume methods for fluid-structure interaction simulation of blood flow in a real stenosed artery. *International Journal of Mechanical Sciences* 2021. Vol. 207 P. 106650. 10.1016/j.ijmecsci.2021.106650
11. E. Nader et al. Blood Rheology: Key Parameters, Impact on Blood Flow, Role in Sickle Cell Disease and Effects of Exercise. *Front. Physiol* 2019. Vol. 10 P. 1329. 10.3389/fphys.2019.01329
12. H. K. Versteeg and W. Malalasekera An Introduction to Computational Fluid Dynamics: The Finite Volume Method. *New York: Wiley* 2007.
13. H. Khawaja and M. Moatamedi Semi-implicit method for pressure-linked equations (SIMPLE) solution in MATLAB. *Int. J. Multiphys* 2018. Vol. 12 P. 313. 10.21152/1750-9548.12.4.313
14. J. L. M. Björkegren and A. J. Lusis Atherosclerosis: Recent developments. *Cell* 2022. Vol. 185 P. 1630–1645. 10.1016/j.cell.2022.04.004

15. L. Saba et al. State-of-the-art CT and MR imaging and assessment of atherosclerotic carotid artery disease: the reporting—a consensus document by the European Society of Cardiovascular Radiology (ESCR). *Eur. Radiol* 2023. Vol. 33 P. 1088–1101. 10.1007/s00330-022-09025-6
16. M. A. Hamidah and S. M. C. Hossain CModeling analysis of pulsatile non-Newtonian blood flow in a renal bifurcated artery with stenosis. *Int. J. Thermofluids* 2024. Vol. 22 P. 100645. 10.1016/j.ijft.2024.100645
17. M. Lou et al. Chinese Stroke Association guidelines for clinical management of cerebrovascular disorders: executive summary and 2019 update on organizational stroke management. *Stroke Vasc. Neurol* 2020. Vol. 5 10.1136/svn-2020-000355
18. M. Malvè, G. Finet, M. Lagache, R. Coppel, R. I. Pettigrew, and J. Ohayon Chapter 10 - Hemodynamic disturbance due to serial stenosis in human coronary bifurcations: a computational fluid dynamics study. *Academic Press* 2021. Vol. 4 P. 225–250. 10.1016/B978-0-12-817195-0.00010-X
19. M. Roy, B. Singh Sikarwar, M. Bhandwal, and P. Ranjan Modelling of Blood Flow in Stenosed Arteries. *Procedia Comput. Sci* 2017. Vol. 115 P. 821–830. 10.1016/j.procs.2017.09.164
20. P. Owasit and S. Sriyab Mathematical modeling of non-Newtonian fluid in arterial blood flow through various stenoses. *Adv. Differ. Equations* 2021. Vol. 1 P. 340. 10.1186/s13662-021-03492-9
21. Pelz DM, Fox AJ, Spence JD, Lownie SP Carotid Stenosis and Stroke: Historical Perspectives Leading to Current Challenges. *Canadian Journal of Neurological Sciences / Journal Canadien des Sciences Neurologiques* 2025. Vol. 52. 10.1017/cjn.2024.40
22. Robert J. Henning, Brian L. Hoh The diagnosis and treatment of asymptomatic and symptomatic patients with carotid artery stenosis. *Current Problems in Cardiology* 2025. Vol. 50 10.1016/j.cpcardiol.2025.102992.
23. S.-K. Jeong and R. S. Rosenson Shear rate specific blood viscosity and shear stress of carotid artery duplex ultrasonography in patients with lacunar infarction. *BMC Neurol* 2013. Vol. 13 P. 36. 10.1186/1471-2377-13-36
24. S. Kumar and S. Kumar Blood Flow with Heat Transfer through Different Geometries of Stenotic Arteries. *Trends Sci* 2023. Vol. 20 P. 6965. 10.48048/tis.2023.6965
25. Ul Haq, U., Ahmed, A., Mustansar, Z., Shaukat, A., Cukovic, S., Nadeem, F., ... Margetts, L. Computational modeling and simulation of stenosis of the cerebral aqueduct due to brain tumor. *Engineering Applications of Computational Fluid Mechanics* 2022. Vol. 16 P. 1018–1030. 10.1080/19942060.2022.2056511
26. W.-J. Tu et al. Estimated Burden of Stroke in China in 2020. *JAMA Netw. open* 2023. Vol. 6 10.1001/jamanetworkopen.2023.1455
27. W. Meng et al. Concentration Polarization of High-Density Lipoprotein and Its Relation with Shear Stress in an In Vitro Model. *J. Biomed. Biotechnol* 2009. P. 695838 10.1155/2009/695838